

GT2011-45043

THE EFFECT OF HEAT GENERATION ON LOW CYCLE FATIGUE LIFE PREDICTION

Onome Scott-Emuakpor¹, Tommy George,
 & Charles Cross
 Air Force Research Laboratory
 Propulsion Directorate
 Wright-Patterson AFB, OH 45433

Todd Letcher, John Wertz,
 & M.-H. Herman Shen
 Departments of Mechanical and Aerospace Engineering
 The Ohio State University
 Columbus, OH 43210

ABSTRACT

An energy-based life prediction method is used in this study to determine the fatigue life of tension-compression loaded components in the very low cycle regime between 10^2 and 10^4 . The theoretical model for the energy-based prediction method was developed from the concept that the strain energy accumulated during both monotonic failure and an entire fatigue process are equal; In other words, the scalar quantity of strain energy accumulated during monotonic failure is a physical damage quantity that correlates to fatigue as well. The energy-based method has been successfully applied to fatigue life prediction of components failing in the fatigue regime between 10^4 and 10^7 cycles. To assess Low Cycle Fatigue (LCF) with the prediction method, a clearer understanding of energy dissipation through heat, system vibration, damping, surface defects and acoustics were necessary. The first of these topics analyzed is heat. The analysis conducted studies the effect of heat generated during cyclic loading and heat loss from slipping at the interface of the grip wedges of the servo-hydraulic load frame and the test specimen. The reason for the latter is to address the notion that slippage in the experimental setup may be the cause of the reduction in the accuracy of the energy-based prediction method for LCF, which was seen in previous research. These analyses were conducted on Titanium 6Al-4V, where LCF experimental data for stress ratios $R=-1$ and $R=-0.813$ were compared with the energy-based life prediction method. The results show negligible effect on both total and cyclic energy from heat generation at the interface of the grip wedges and heat generation in the fatigue zone of the specimen.

NOMENCLATURE

A_1 Temperature approximation slope for $T1$
 A_2 Temperature approximation slope for $T2$
 B_1 Temperature approximation constant for $T1$

B_2 Temperature approximation constant for $T2$
 C Material parameter for cyclic strain
 C_p Material specific heat
 E Modulus of elasticity
 N Loading cycle
 N_f Number of cycles to failure
 R Alternating stress ratio (min versus max stress)
 $T1$ Temperature during fatigue: $+0 < N/N_f < 0.92$
 $T2$ Temperature during fatigue: $0.92 < N/N_f < 1$
 W_c Strain energy density per cycle
 W_f Monotonic strain energy density
 W_N General monotonic strain energy density
 W_{Temp} Heat generated energy density during fatigue

β_1 Monotonic stress regression slope
 β_2 Monotonic stress regression constant
 ΔT Change in temperature
 ΔT_m Monotonic tensile temperature change
 ϵ Monotonic strain
 ϵ_{cycle} Peak-to-peak cyclic strain
 ϵ_{mean} Mean strain
 ϵ_n Ultimate tensile strain
 ϵ_o Material parameter for monotonic strain
 ρ Material Density
 σ Nominal monotonic stress
 σ_a Stress amplitude
 σ_c Material parameter for cyclic strain
 σ_{mean} Mean stress
 σ_n Ultimate tensile stress
 σ_o Material parameter for monotonic strain
 σ_{PP} Peak-to-Peak cyclic stress
 σ_y Yield stress

¹ Corresponding author. Tel.: +1-937-255-6810; fax: +1-937-656-5532
 E-mail address: onome.scott-emuakpor@wpafb.af.mil (Onome Scott-Emuakpor)

1. INTRODUCTION

Modern gas turbine engines are designed to perform more efficiently than their predecessors. In other words, the requirements for thrust, fuel efficiency, emission and noise reduction are becoming more demanding while engines are getting smaller, with respect to size and parts count. This has resulted in turbine disks experiencing a significant increase in thermal-mechanical loading during transitional flight cycles. These extreme loading environments are key causes of Low Cycle Fatigue (LCF) in turbine disks [1]. The LCF problem, however, is not limited to only large scale gas turbine engines; since small turbines transmit considerable amounts of energy per pound of material, the rotating assembly is subjected to many different stress states [2]. Despite the fact that these stress states often result in LCF, the issue is underemphasized during analysis of small turbine structural problems and negligence could lead to rotor bursts [2]. Based on the fatigue issues in gas turbine engines, it is desired to develop a LCF assessment method as a benchmark model for evaluating turbine engine disks.

The assessment method of choice for LCF is the energy-based life prediction method [3]. This lifing model was developed from the understanding that the energy accumulated in a monotonic failure process is a physical damage quantity with a value equal to the energy accumulated during fatigue to failure; therefore, failure cycles can be determined by dividing the monotonic energy by the average energy per cycle in a fatigue process [4, 5].

Since it has been determined in a previous study that energy accumulated through heat, system vibration, damping, surface defect and acoustics are negligible in the irreversible damaging process of fatigue [6], the total monotonic strain energy is the only energy value that makes up the physical damage quantity used in the energy-based method. With this theory in place, the energy-based life prediction method has been compared, with encouraging results, to experimental failure data for axial tension-compression, uniaxial and biaxial bending in the fatigue regime of 10^4 - 10^7 cycles [3, 7, 8]. LCF comparisons below 10^4 cycles, however, showed less appealing results. One of the assumed causes of inaccurate LCF assessment was the possibility of specimen slipping at the wedges of the experimental test setup [7]. If this assumption were true, it would reduce plastic deformation per cycle during fatigue loading, making fatigue failure longer than anticipated and, therefore, the LCF prediction would be underestimated. In an effort to improve this comparison, re-examining the effects of all energy accumulated during cyclic loading is proposed.

The following sections focus on energy generated by heat in each failure process. Due to large applied loads and large strains, it is assumed that a majority of heat in each mechanical process will occur from heat generation at the fatigue zone and slippage of the test specimen from the hydraulic grips of the servo-hydraulic axial testing device. This assumption was analyzed in detail for Titanium 6Al-4V (Ti 6Al-4V) material.

2. EXPERIMENTAL PROCEDURES

Several experiments were carried out in order to perform a thorough investigation of the heat effects in Ti 6Al-4V fatigue and monotonic fracture data. The experiments consists of tension-compression fatigue to failure tests at 5 Hz, monotonic tensile tests and tension-compression cyclic loading tests, not to failure, at 0.1 Hz. Each of these tests is conducted on a 100KN MTS (Material Testing System) servo-hydraulic axial load frame. All mechanical properties and data acquired from each test are done so using a MTS TestStarIIs controller and an extensometer, which is a strain measurement instrumentation. Thermal properties of each test were acquired using K-type thermal couples with two 10-channel Omega monogram controllers. The thermal readings were used to measure the heat generated from friction at the interface of the grip wedges and the heat generated in the fatigue section of the specimen. All tests were conducted at room temperature.

The specimens used for each experiment were machined by a water-jet process without a delicate surface finishing procedure. The specimens were cut from a 3.175mm thick plate stock of Ti 6Al-4V. The monotonic tensile specimens were made according to ASTM (American Society of Testing and Materials) E8 standard [9]. The fatigue specimens, which were made according to ASTM standard E466, utilize two different geometries: (1) a continuous radius specimen and (2) a uniform gage-section specimen, both shown in Fig. 1 [10]. When compared to the geometry of the uniform gage-section specimen, the continuous radius specimen was less susceptible to buckling at higher compressive stress magnitudes. The uniform gage-section, however, is more compatible with the use of the extensometer because they both have the same gage length (25.4mm); thus, it allows for more precise hysteresis results during the cyclic loading tests at sub 1 Hz frequencies. Though, according to ASTM standard E466, it is fair to assume the fatigue characteristics of the continuous radius and the uniform gage-section specimens are the same, the comparison was still observed, experimentally.

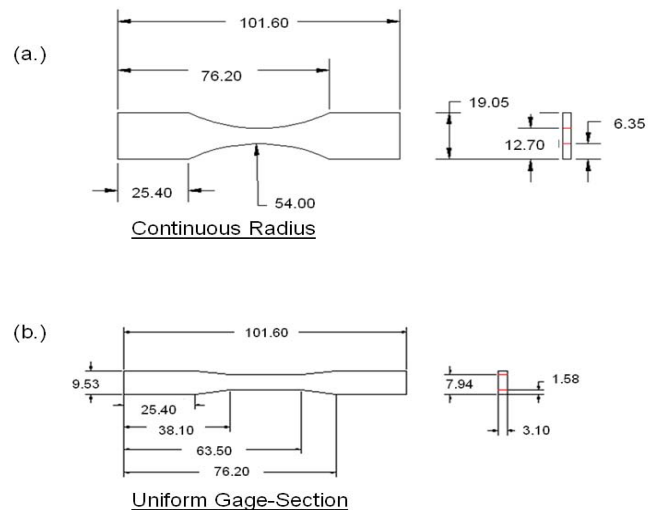


Fig 1. ASTM fatigue specimens: (a.) Continuous radius, (b.) uniform gage-section.

3. ENERGY-BASED LIFE PREDICTION METHOD

The energy-based fatigue life calculation method was developed from the stress-strain representations for monotonic and cyclic loading behaviors shown in Eq. (1)-(3). Equation (1) and (2) represent the respective monotonic stress-strain relationship prior to and after the necking phenomenon, and Eq. (3) is the expression for the cyclic strain [3, 5]. Equation (3) was created based on a simplified coordinate system, where the horizontal versus vertical axes represents peak-to-peak strain versus peak-to-peak stress, respectively. On this coordinate system, shown in Fig. 2, the origin is defined as the minimum fully-reversed point of a hysteresis loop; in other words, both the stress and the strain values are read from zero to peak-to-peak magnitudes.

$$\varepsilon = \frac{\sigma}{E} + \varepsilon_o \sinh\left(\frac{\sigma}{\sigma_o}\right) \quad (1)$$

$$\sigma = \beta_1 \varepsilon + \beta_o \quad (2)$$

$$\varepsilon_{cycle} = \frac{\sigma_{pp}}{E} + \frac{1}{C} \sinh\left(\frac{\sigma_{pp}}{\sigma_c}\right) \quad (3)$$

The parameters for Eq. (1)-(3) are defined as follows: σ is the nominal applied monotonic stress value, ε is the strain corresponding to the applied monotonic stress, β_1 & β_o are the respective slope and intercept of the stress-strain relationship in the necking region (From ultimate tensile to point of fracture), σ_{pp} is the generalized/peak-to-peak stress value corresponding to the generalized/peak-to-peak cyclic strain ε_{cycle} ($2\sigma_a$ replaces σ_{pp} in Eq. (3) after all necessary derivations), E is the modulus of elasticity, and the variables σ_c , σ_o , ε_o , and C are curve fit parameters [3]. The curve fit parameters for the cyclic and monotonic representations are statistically acquired by comparison between the equations and the respective experimental results.

The energy-based prediction method calculates fatigue life by taking the total monotonic strain energy density and dividing it by the strain energy density for one cycle. The total strain energy density accumulated during a monotonic process is determined as the area underneath the curve constructed by Eq. (1) & (2), and the strain energy density for one cycle is represented by the area within the hysteresis loop formed by Eq. (3). Calculating the monotonic strain energy density from experimental results is a straightforward task, whereas the strain energy density in one cycle is determined by making a simplification-based assumption that the tensile stress-strain behavior of the hysteresis loop is the same as the compressive behavior. This assumption is essentially a simplification for the strain energy density per cycle calculation because Bauschinger effect shows that the tensile and compressive behaviors in a hysteresis loop are not identical [11]. The effect of the simplification is unknown but assumed to be minor. Cyclic strain energy density can be determined by the Eq. (4) expression.

$$W_c = \sigma_{pp} \varepsilon_{cycle} - 2 \int_0^{\sigma_{pp}} \varepsilon_{cycle} d\sigma_{pp} \quad (4)$$

The assumed effects of introducing a positive mean stress to a cyclic loading process are as follows: a reduction in the physical damage quantity and an increase in the strain energy density per cycle [7]. The damage quantity is reduced because the mean stress is viewed as a static stress; thus, the mean/static strain energy density is subtracted from the monotonic strain energy density. The increase in the strain energy density per cycle is based on a shift of the stress-strain behavior along both the peak-to-peak stress and strain axes of the simplified hysteresis coordinate system; meaning, cyclic loads with stress ratios greater than -1 experience more plastic deformation than their fully-reversed counterpart. Applying these mean stress effects to the principles of the energy-based life prediction method results in shorter fatigue life data than the fully-reversed case. An illustration of the mean stress effect can be seen in Fig. 3; the corresponding strain energy density equations are expressed by Eq. (5)-(9).

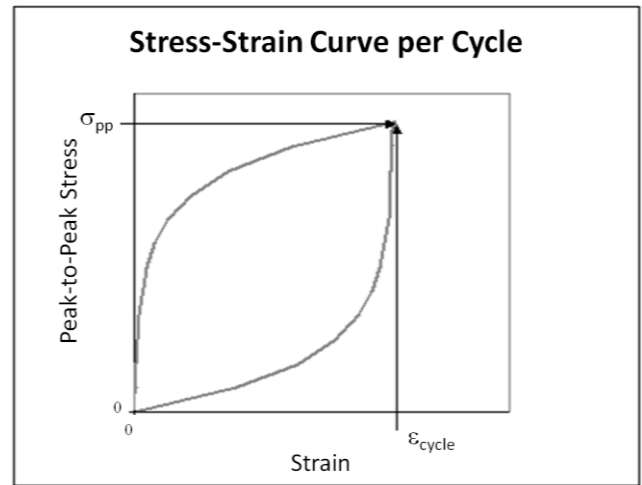


Fig. 2. Energy-based hysteresis schematic, simplified coordinates.

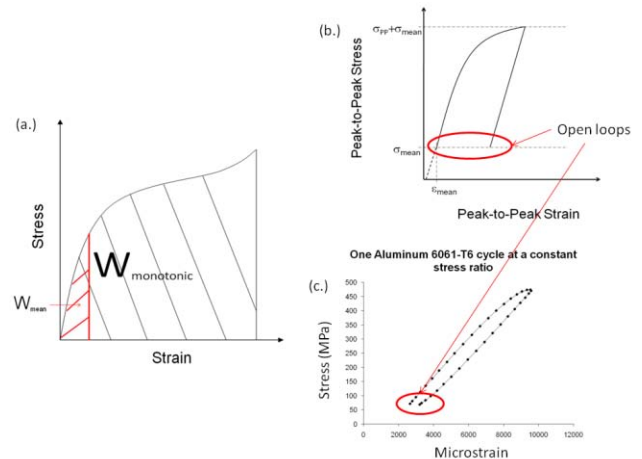


Fig. 3. Energy-based means stress effect: (a.) monotonic schematic, (b.) cyclic schematic, (c.) experimental hysteresis results (Aluminum 6061-T6).

$$W_N = W_f - \left[\sigma_{mean} \left(\varepsilon_{mean} - \frac{\sigma_{mean}}{2E} \right) - \varepsilon_o \sigma_o \left(\cosh \left(\frac{\sigma_{mean}}{\sigma_o} \right) - 1 \right) \right] \quad (5)$$

$$W_c = \sigma_{pp} \left(\varepsilon_{cycle} + \varepsilon_{mean} \right) - \int_{\sigma_{mean}}^{\sigma_{pp} + \sigma_{mean}} d\sigma_{pp} - \int_0^{\sigma_{pp}} d\sigma_{pp} \quad (6)$$

$$\sigma_{pp} \left(\varepsilon_{cycle} + \varepsilon_{mean} \right) = 2\sigma_a \left[\frac{2\sigma_a + \sigma_{mean}}{E} + \frac{\sinh \left(\frac{2\sigma_a + \sigma_{mean}}{\sigma_c} \right)}{C} \right] \quad (7)$$

$$\int_{\sigma_{mean}}^{\sigma_{pp} + \sigma_{mean}} d\sigma_{pp} = \frac{1}{2EC} \left[\begin{aligned} & (2\sigma_a + \sigma_{mean})^2 C + 2\sigma_c \cosh \left(\frac{2\sigma_a + \sigma_{mean}}{\sigma_c} \right) E \\ & - \sigma_{mean}^2 C - 2\sigma_c \cosh \left(\frac{\sigma_{mean}}{\sigma_c} \right) E \end{aligned} \right] \quad (8)$$

$$\int_0^{\sigma_{pp}} d\sigma_{pp} = \frac{-\sigma_o E + 2\sigma_a^2 C + \sigma_o \cosh \left(\frac{2\sigma_a}{\sigma_o} \right) E}{EC} \quad (9)$$

4. RESULTS AND DISCUSSION

4.1. Experimental Results

Following ASTM E8 standard, four monotonic tensile-to-fracture tests were conducted on Ti 6Al-4V flat dog-bone specimens using the MTS servo-hydraulic load frame under a controlled displacement rate of 2.54E-2 mm/s. These tests were conducted in order to determine the total monotonic strain energy density, which is the value used for the physical damage quantity in the conventional energy-based life prediction method of specimens experiencing uniform stress distribution through the volume of the fatigue zone. The material data necessary for strain energy density determination are the elastic modulus (E), ultimate tensile stress (σ_n), yield stress (σ_y), and the percent elongation.

The results of the monotonic tensile tests were compared graphically and statistically on Fig. 4 and Table 1, respectively. The statistical comparison in the table is made by analyzing the relative standard deviation of each material property. The results of both comparisons provide confidence in the acquired material properties. Based on minimal variation in the comparison, the average value of each material property was used to determine the total monotonic strain energy density necessary for life prediction. These results are presented in Table 2.

Table 1. Standard deviation results from monotonic tests.

Properties	STD	Relative STD (Unit %)
E (MPa) =	1577	1.44
σ_n (MPa) =	9.189	0.87
σ_y (MPa) =	6.403	0.63
Elongation (%) =	0.244	1.46

Table 2. Average material property results.

Properties	Average
E (MPa) =	109442
σ_n (MPa) =	1051
σ_y (MPa) =	1010
Elongation (%) =	16.69
W_f (MJ/m ³) =	557

Monotonic Experimental Results: Ti 6Al-4V

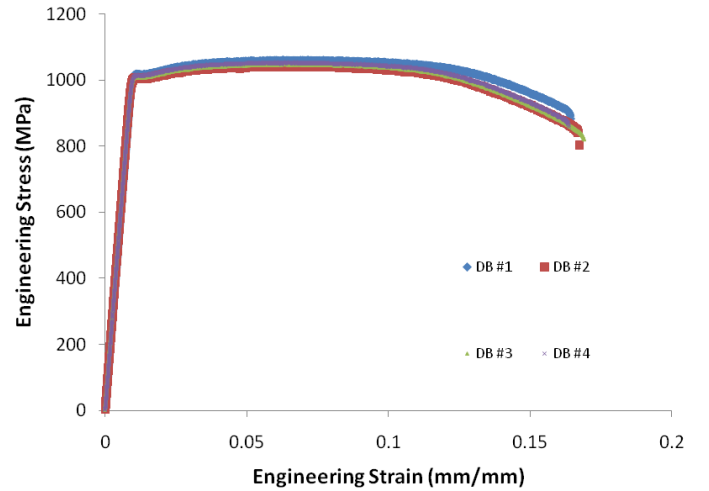


Fig. 4. Monotonic tensile data: Ti 6Al-4V.

The experimental goal for LCF analysis was to acquire a sufficient amount of data, with a failure criterion of complete fracture, between 10^2 - 10^4 cycles. Fatigue data between 10^3 - 10^4 cycles was capable via a basic fully-reversed ($R=-1$) cyclic load, where the fatigue data point with the shortest life span failed at approximately 2×10^3 cycles. Due to buckling from excessive heat generation in the fatigue zone, acquiring fatigue data between 10^2 - 10^3 cycles was a challenge. Therefore, a stress ratio of $R=-0.813$ was chosen in order to maintain the maximum allowable compressive stress magnitude yet apply a greater tensile stress magnitude than the compressive value. Fatigue data at $R=-1$ and $R=-0.813$ were acquired from the continuous radius specimen and the uniform gage-section specimen. A similarity analysis was conducted on the fatigue behavior of the two geometries to verify ASTM E466 standard. The similarity of the behaviors is verified by the graphical comparison of alternating stress versus cycle (S-N) data shown on Fig. 5, where the operating frequency for all the data points is 5 Hz. The failure mode of the uniform gage-section geometry at $R=-0.813$ between 10^2 - 10^3 cycles is buckling. Nonetheless, the fatigue life comparison with fatigue data of the continuous radius specimen, whose failure mode is complete fracture, still validates the ASTM E466 standard.

Specimen Geometry Fatigue Comparison: Ti 6Al - 4V

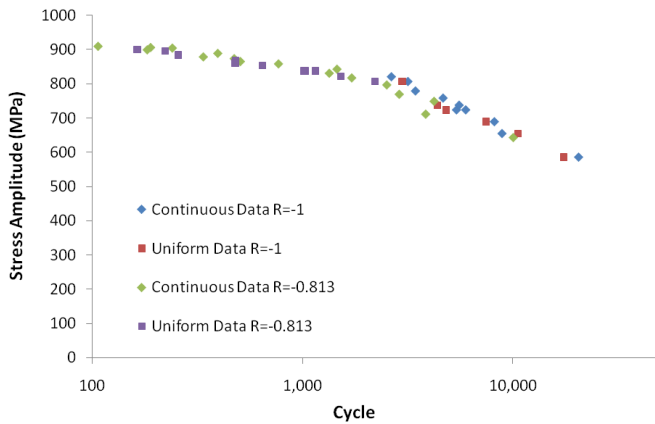


Fig. 5. Ti 6Al-4V fatigue data comparison.

Previously stated in Section 2, the uniform gage-section specimen is used to acquire hysteresis stress-strain results at a loading frequency of 0.1 Hz. This specimen is chosen over the continuous radius specimen because it has the same gage length as the extensometer (25.4mm). Following the procedure from previous research, the saturated strain energy density during a fatigue process can be observed as the average strain energy density in the entire process [12]. Previous research also concludes that the strain energy density saturation will occur between 20% and 70% of the cycles to failure [12]. Therefore, hysteresis data was acquired for 500 cycles, beginning at 40% of the anticipated cycles to failure for a stress amplitude of 691 MPa. The strain energy density per cycle result of this experiment is plotted on Fig. 6. The optimized saturated cyclic strain energy density value and its material parameters (σ_c , C) are shown in Table 3. The results in the table were chosen based on a recently proposed statistical optimization curve fit procedure, which observes the error-estimate of each experimental data point versus Eq. (3) and extracts outlier data points before using several iterations to determine the optimal material parameters [13].

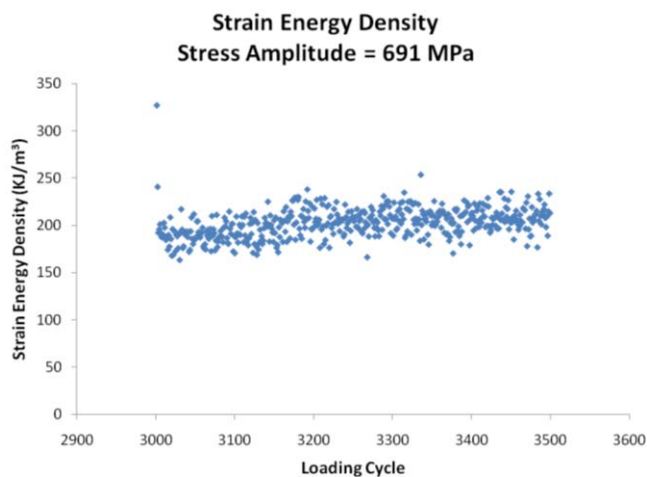


Fig. 6. Strain energy density per cycle: Ti 6Al-4V.

Table 3. Hysteresis material parameters.

Properties for 691MPa	Optimal Values
σ_c (MPa)=	201
C (mm/mm) =	2.00E+07
W_c (KJ/m ³) =	202

4.2. Energy Dissipation Through Heating

Stated previously, the accuracy of LCF prediction below 10^4 cycles isn't as appealing as HCF predictions [7]. Since this inaccuracy was attributed to slippage between the wedges and the test specimen, the heat generated at the interface between the hydraulic-grip wedges and the test specimen was analyzed. Also analyzed was the heat generated in the specimen's fatigue zone. The first of the two topics addressed was heat generated at the interface of the grip wedges. The temperature was measured with thermal couples at the interface of both the upper and the lower grips during a fatigue process (Fig. 7), where the initial temperature reading, which was converted from Degrees Fahrenheit to Kelvin with the expression $(T-32)/(5/9)+273.15$, was 296.9K and 295.3K (74.8F and 71.8F), respectively. The results for the temperature change at each grip showed a ΔT of approximately 0 degrees Kelvin; thus verifying no friction between the specimen and the clamped surfaces.



Fig. 7. Test set up of wedge and thermal couple.

In the case of heat produced by plastic work, temperature increase in the fatigue zone of a specimen was recorded for both the monotonic and the cyclic loading case. Temperature data was collected every 10 seconds during monotonic fracture process whereas temperature during cyclic loading was recorded at specific loading cycles during the fatigue process. The data for a single monotonic test and a single fatigue test are shown in Table 4 and 5, respectively. The data from Table 4 was used to create the temperature change versus engineering strain plot shown in Fig. 8. The figure shows that heat generation is purely attributed to plastic work in the system, which begins at a strain of approximately $1E-2$. Note, the larger the plastic work the greater the heat generated in the system. This understanding is shown visually on the plot of temperature change versus normalized cycle (N/N_f , failure value = 1) in Fig. 9. This figure shows limited change in temperature until the

loading cycles approach fatigue failure, a region where plastic work increase drastically compared to most of the process [4].

Table 4. Temperature during monotonic fracture.

Time (Sec)	Strain (mm/mm)	Temperature (K)
0	5.036E-05	295.93
10	3.206E-03	295.82
20	6.064E-03	295.71
30	8.602E-03	295.43
40	1.486E-02	295.59
50	2.310E-02	297.32
60	3.139E-02	298.43
70	3.986E-02	299.82
80	4.837E-02	300.54
90	5.709E-02	301.48
100	6.604E-02	302.32
110	7.499E-02	303.09
120	8.411E-02	303.87
130	9.330E-02	304.54
140	1.029E-01	305.59
150	1.125E-01	305.93
160	1.225E-01	306.26
170	1.327E-01	306.98
180	1.433E-01	307.26
190	1.539E-01	308.15
200	1.643E-01	308.48

$$\Delta T_m = 12.55$$

Table 5. Temperature during fatigue: $\sigma_a = 806$ MPa.

Cycles	Temperature (K)
0	294.65
119	294.82
300	295.26
450	295.43
600	295.59
750	295.76
900	296.04
1100	296.09
1250	296.32
1400	296.65
1550	297.09
1700	298.26
1800	300.26
1900	307.71
1912	315.93

Monotonic Temperature Analysis: Ti 6Al-4V

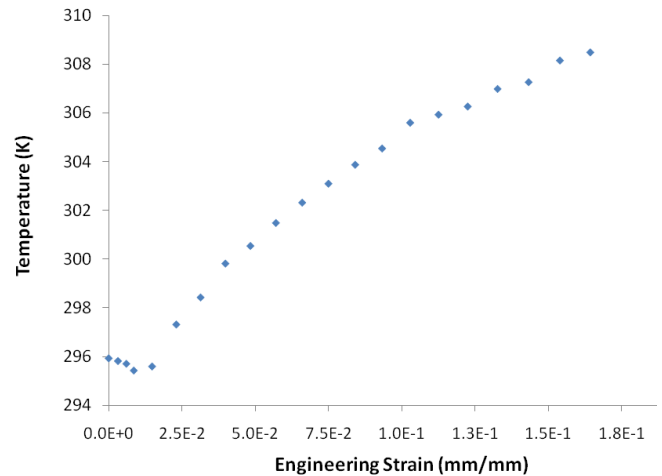


Fig. 8. Temperature versus engineering strain during monotonic fracture.

Temperature Analysis Fatigue: Ti 6Al-4V, $\sigma_a = 806$ MPa

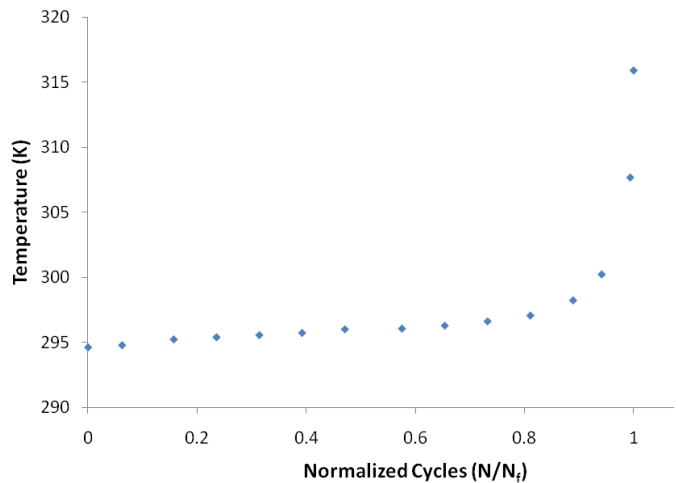


Fig. 9. Temperature versus normalized loading cycles (N/N_f).

In order to determine the cyclic energy density dissipation due to heat generation, a general equation of the temperature trend throughout a fatigue process was necessary. This trend, which is assumed to be the same at all LCF loading stresses, is acquired by observing the temperature behavior in Fig. 9. As shown in Fig. 10, this behavior can be characterized by two linear approximations. The approximations are represented by Eq. (10) and (11). Note that the normalized loading cycle where Eq. (10) and (11) intersect ($N/N_f \approx 0.92$) is consistent with the critical energy percent of cycles to failure found in previous energy-based research [14]. The resulting energy density dissipation via heat for an entire fatigue process is represented by Eq. (12). The values for the material properties and equation parameters for Eq. (10)-(12) are shown in Table 6.

Temperature Analysis Fatigue: Ti 6Al-4V,
 $\sigma_a=806\text{MPa}$

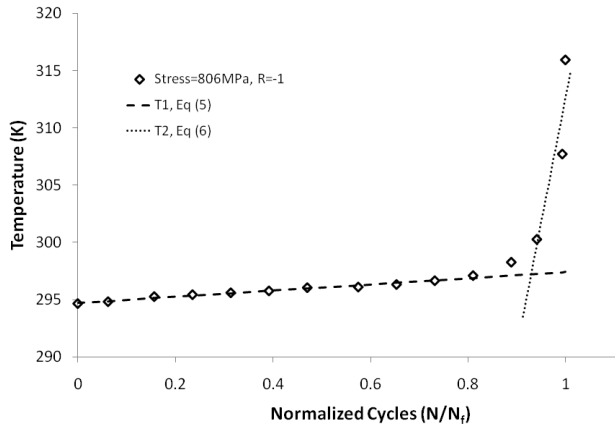


Fig. 10. Linear approximations of temperature behavior during fatigue.

$$T1 = A_1 \left(\frac{N}{N_f} \right) + B_1 \quad (10)$$

$$T2 = A_2 \left(\frac{N}{N_f} \right) + B_2 \quad (11)$$

$$W_{Temp} = \rho C_p [0.92A_1 + 0.08A_2] \quad (12)$$

Table 6. Material properties for Eq. (10)-(12).

Material Properties	
A_1 (K)	2.6992
B_1 (K)	294.71
A_2 (K)	218.92
B_2 (K)	93.773
ρ (kg/m ³)	4500
C_p (J/kg-K)	522

4.3. Energy-Based Life Prediction with Heat Effect

As stated in Section 1, failure cycles can be determined by taking the monotonic strain energy density value and dividing it by the average strain energy density per cycle in a fatigue process. The strain energy density, which is the area underneath the true stress-strain curve constructed by Eq. (1) and (2), is given as the damage quantity W_f in Table 2; W_f is used for fully-reversed cases only. The damage quantity in a general case (W_N), which could include a mean stress effect, is expressed by Eq. (5). Therefore, dividing W_N by Eq. (6), which is the average strain energy density per cycle in a general case (W_c), gives a prediction of life with respect to alternating and mean stresses. The life prediction is compared with experimental results for $R=-1$ and $R=-0.813$ in Fig. 11. As seen in comparisons from previous research, the results show a discrepancy between the experimental results and the prediction. The first attempt to closing the gap of this comparison calls for observing the effect of heat generation to the energy-based life prediction method.

Fatigue Comparison: Ti 6Al-4V

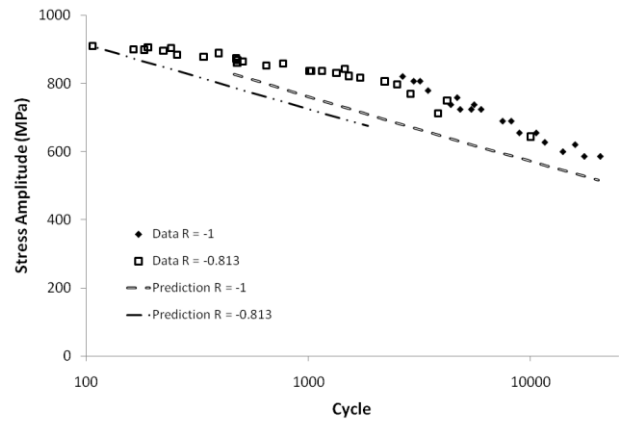


Fig. 11. Fatigue life prediction and comparison.

The analyzed energy in a test specimen under mechanical loading is plastic work plus work from temperature rise at the surface of the specimen. Using the general energy-based equations, the total energy in a monotonic fracture process is expressed by Eq. (13) and the energy in a fatigue process is Eq. (14). Therefore, cycles to failure (N_f) is represented by Eq. (15). The curve of Eq. (15) is plotted and compared with experimental data and the energy-based life prediction without heat generation effect on Fig. 12 and 13 for $R=-1$ and $R=-0.813$, respectively. This comparison is also shown with the fully-reversed continuous radius data in Table 7. Both comparisons show a negligible effect on the prediction method when accounting for the heat generated in the mechanical loading system.

$$W_N + \rho C_p \Delta T_m \quad (13)$$

$$\left[W_c + \rho C_p \left(\frac{A_1}{N_f} \right) \right] 0.92 N_f + \left[W_c + \rho C_p \left(\frac{A_2}{N_f} \right) \right] 0.08 N_f \quad (14)$$

$$N_f = \frac{W_N + \rho C_p (\Delta T_m - 0.92A_1 - 0.08A_2)}{W_c} \quad (15)$$

Fatigue Comparison for R = -1: Ti 6Al-4V

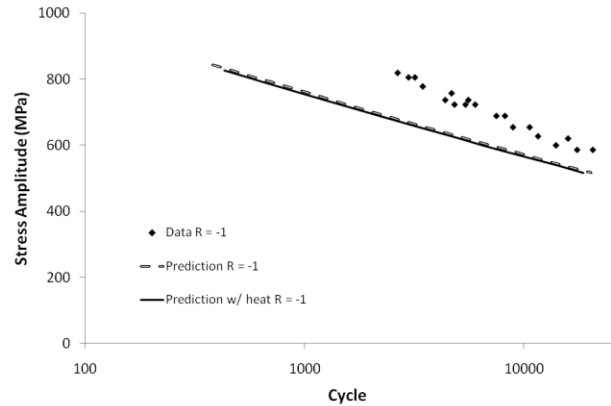


Fig. 12. Fatigue life prediction and comparison, $R=-1$.

Fatigue Comparison for R = -0.813: Ti 6Al-4V

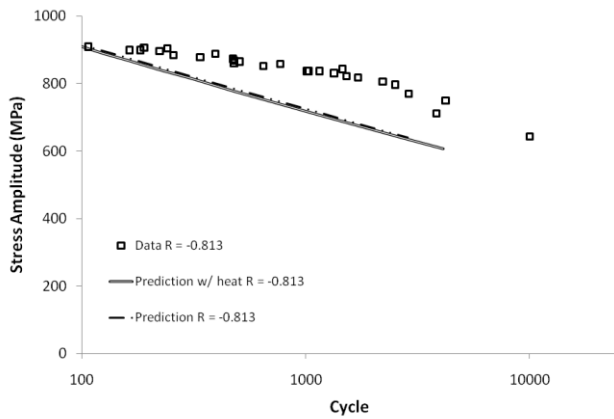


Fig. 13. Fatigue life prediction and comparison, $R=-0.813$.

Table 7. Fatigue life comparison for continuous radius specimen

Amplitude Stress (MPa)	Data Cycles	Prediction Cycles	Prediction w/Heat Cycles
724	5401	1561	1443
806	3179	591	546
724	5978	1561	1443
820	2653	504	466
655	8883	3572	3303
586	20517	8360	7731
779	3451	815	754
758	4667	1039	960
737	5564	1325	1226
689	8167	2355	2178
620	15817	5447	5037

5. CONCLUSION

The effect of heat on tension-compression loaded specimens was analyzed and applied to the energy-based prediction method to determine LCF between 10^2 - 10^4 cycles. Two key results were found from the analysis. First, the test setup showed no significant signs of slipping at the grip-specimen interface. Second, the change in surface temperature at the fatigue zone of the mechanically loaded specimen generates an insignificant energy value compared to the plastic work (strain energy density) in the system. The negligible effect of heat during mechanical loading is shown by the comparisons of the energy-based prediction calculations with and without energy from heat.

As a result of the analysis conducted in the previous sections, future work will be in the following two areas: (1) determining if the energy accumulated via system vibration, damping, surface defects and acoustics contributes to the damaging factor required to fail a component, and (2) improving the LCF life prediction capability of the energy-based method.

ACKNOWLEDGEMENTS

The authors would like to thank the Air Force Research Laboratories (AFRL), specifically the Turbine Engine Fatigue Facility (TEFF) and the Air Force Office of Scientific Research (AFOSR) for their funding and support.

REFERENCE

- [1] Karimbaev, K., and Servetnik, A., "Low-Cycle Fatigue Life Assessment for Gas Turbine Engine Disks under Flight Cycle Conditions," *Journal of Strength of Materials*, 2009, Vol. 41, Issue 1, pp. 102-105.
- [2] Sorenson, G., and Clemett, H., "Low-Cycle Fatigue in Small Turbines," *Journal of Experimental Mechanics*, 1962, Vol. 2, Issue 12, pp. 353-358.
- [3] Scott-Emuakpor, O., Shen, M.-H.H., George, T., Cross, C., and Calcaterra, J., "Development of an Improved High Cycle Fatigue Criterion," *Journal of Engineering for Gas Turbines and Power*, 2007, Vol. 129, Issue 1, pp. 162-169.
- [4] Feltner, C.E., and Morrow, J.D., "Microplastic Strain hysteresis Energy as a Criterion for Fatigue Fracture," *Journal of Basic Engineering Transactions, American Society of Mechanical Engineers*, New York, 1961, Vol. 83, pp. 15-22.
- [5] Stowell, E., "A Study of the Energy Criterion for Fatigue," *Nuclear Engineering and Design*, 1966, Vol. 3, pp. 32-40.
- [6] Xiao-Yan, T., De-Jun, W., and Hao, X., "Investigation of Cyclic Hysteresis Energy in Fatigue Failure Process," *International Journal of Fatigue*, 1989, Vol. 11, No. 5, pp 353-359.
- [7] Scott-Emuakpor, O., Shen, M.-H.H., George, T., and Cross, C., "An Energy-Based Uniaxial Fatigue Life Prediction Method for Commonly Used Gas Turbine Engine Materials," *Journal of Engineering for Gas Turbines and Power*, 2008; Vol. 130, Issue 6, pp. 062504-1.
- [8] Scott-Emuakpor, O., Shen, M.-H.H., George, T., and Cross, C., "Multi-Axial Fatigue Life Prediction via a Strain Energy Method" *AIAA Journal*, 2010; Vol. 48, No. 1, pp. 63-72
- [9] American Society for Testing and Materials, "E8M-09: Standard Test Methods for Tension Testing of Metallic Materials," *ASTM Book of Standards*, 2009; Vol. 03.01, ASTM International, West Conshohocken, PA.
- [10] American Society for Testing and Materials, "E466-07: Standard Practice for Conducting Force Controlled Constant Amplitude Axial Fatigue Tests of Metallic Materials," *ASTM Book of Standards*, 2009; Vol. 03.01, ASTM International, West Conshohocken, PA.
- [11] Panontin, T., and Sheppard, S., "Fatigue and Fracture Mechanics," *ASTM, STP-1332*, 1999; Vol. 29, ASTM International, West Conshohocken, PA.

[12] Scott-Emuakpor, O., George, T., Cross, C., and Shen, M.-H.H., "Hysteresis Loop Representation for Strain Energy Calculation and Fatigue Assessment," *Journal of Strain Analysis for Engineering Design*, 2010, Vol. 45, Issue 4, pp. 275-282.

[13] Scott-Emuakpor, O., George, T., Cross, C., and Shen, M.-H.H., "Analysis of Strain Energy Behavior throughout a Fatigue Process," *Journal of Experimental Mechanics*, Accepted for Journal Publication, 2010.

[14] Ozaltun, H., Shen, M-MH, George, T., and Cross, C. "Hysteresis-loop representation for strain energy calculation and fatigue assessment," *Journal of Strain Analysis for Engineering Design*, Vol 45, number 4, pp 275-282, 2010.